NUCLEAR THEORY, Vol. 40 (2023)
eds. M. Gaidarov, N. Minkov, Heron Press, Sofia

Charge- and Neutral-Current Quasielastic (Anti)Neutrino Scattering on ^{12}C Target with Realistic Spectral and Scaling Functions

M.V. Ivanov[1], **A.N. Antonov**[1], **M.B. Barbaro**[2,3], **J.A. Caballero**[4], **G.D. Megias**[4], **R. González-Jiménez**[5], **C. Giusti**[6], **A. Meucci**[6], **E. Moya de Guerra**[5], **J.M. Udías**[5]

[1]Institute for Nuclear Research and Nuclear Energy, Bulgarian Academy of Sciences, Sofia 1784, Bulgaria

[2]Università di Torino, Dipartimento di Fisica, I-10125 Turin, Italy

[3]Istituto Nazionale di Fisica Nucleare, Sezione di Torino, I-10125 Turin, Italy

[4]Departamento de Física Atómica, Molecular y Nuclear, Universidad de Sevilla, 41080 Sevilla, Spain

[5]Grupo de Física Nuclear, Departamento de Estructura de la Materia, Física Térmica y Electrónica, Facultad de Ciencias Físicas, Universidad Complutense de Madrid and IPARCOS, CEI Moncloa, Madrid 28040, Spain

[6]Dipartimento di Fisica, Università degli Studi di Pavia and INFN, Sezione di Pavia, via Bassi 6 I-27100 Pavia, Italy

Abstract. Charge-current (CC) and neutral-current (NC) quasielastic (anti)neutrino scattering cross sections on ^{12}C target are analyzed using a realistic spectral function $S(p, \mathcal{E})$ that gives a scaling function in accordance with the (e, e') scattering data. The spectral function accounts for the nucleon-nucleon correlations and has a realistic energy dependence. The standard value of the axial mass $M_A = 1.03$ GeV is used in the calculations. The role of the final-state interaction on the spectral and scaling functions, as well as on the cross sections is accounted for. Our results in the CC case are compared with an improved version of the SuperScaling Approach (SuSA), called SuSAv2, as well as with those of the relativistic mean field and the relativistic Green's function in the NC case. Theoretical predictions including both the QE and the 2p-2h meson exchange currents (MEC) contributions are in good accord with the data in most of the kinematical situations explored in the MiniBooNE and Minerνa experiments. The NC results are compared with the empirical data of the MiniBooNE and BNL experiments. The possible missing ingredients in the considered theoretical methods are discussed.

1 Introduction

Having a good understanding of neutrino properties is presently one of the highest priorities in fundamental physics, explaining why considerable effort has

been expended in recent years by a large number of researchers. Most of the recent (MiniBooNE, T2K, MINERνA, NOνA) and future (DUNE, HyperK) long baseline neutrino experiments make use of complex nuclear targets. Hence, precision measurement of neutrino oscillation parameters and the charge-parity (CP) violation phase requires one to have excellent control over medium effects in neutrino-nucleus scattering. In fact, nuclear modeling has become the main issue in providing neutrino properties with high accuracy. A detailed report on the study of neutrino-nucleus cross sections is presented in the NuSTEC White Paper [1].

The aim of the present paper (see also Refs. [2–4]) is to continue our analysis of CC and NC quasielastic (anti)neutrino scattering cross sections on ^{12}C target using the results obtained in Refs. [2, 5] for a realistic spectral function $S(p, \mathcal{E})$ instead of the phenomenological SuSA approach. In this work, in the case of CC anti(neutrino) scattering, we include the fully relativistic weak (with vector and axial components) charged meson-exchange currents, in both longitudinal and transverse channels. These have been evaluated in [6–8] from an exact microscopic calculation, where the two-body current is the sum of seagull, pion-in-flight, pion-pole, and Δ-pole operators and the basis wave functions are noninteracting Dirac spinors.

2 General Formalism

In most neutrino experiments the interaction of the neutrino occurs with nucleons bound in nuclei. The analyses of such processes within different methods involve various effects such as nucleon-nucleon (*NN*) correlations, the final state interactions (FSI), possible modifications of the nucleon properties inside the nuclear medium and others. These effects, however, cannot be presently accounted for in an unambiguous and precise way, and what is very important, in most cases they are highly model-dependent. A possible way to avoid the model-dependencies is to use the nuclear response to other leptonic probes, such as electrons, under similar conditions to the neutrino experiments. The SuSA approach follows this general trend. The analyses of superscaling phenomena observed in electron scattering on nuclei have led to the use of the scaling function directly extracted from (e, e') data to predict (anti)neutrino-nucleus cross sections [9], just avoiding the usage of a particular nuclear structure model. A "superscaling function" $f(\psi)$ has been extracted from the data by factoring out the single-nucleon content of the double-differential cross section and plotting the remaining nuclear response versus a scaling variable $\psi(q, \omega)$ (q and ω being the momentum transfer and transferred energy, respectively). For high enough values of the momentum transfer (roughly $q > 400$ MeV) the explicit dependence of $f(\psi)$ on q is very weak at transferred energies below the quasielastic peak (scaling of the first kind). Scaling of second kind (*i.e.* no dependence of $f(\psi)$ on the mass number A) turns out to be excellent in the same region. The term "superscaling" means the occurrence of both first and second types of scaling.

In this work we consider three different theoretical calculations. Two of them, denoted as HO (harmonic oscillator) and NO (natural orbitals), make use of a spectral function $S(p, \mathcal{E})$, p being the momentum of the bound nucleon and $\mathcal{E}$ the excitation energy of the residual nucleus, coinciding with the missing energy E_m up to a constant offset [10]. The area of analyses of the scaling function, the spectral function, and their connection (see, *e.g.*, Refs. [5, 11]) provides insight into the validity of the mean-field approximation (MFA) and the role of the *NN* correlations, as well as into the effects of FSI. Though in the MFA it is possible, in principle, to obtain the contributions of different shells to $S(p, \mathcal{E})$ and $n(p)$ for each single-particle state, owing to the residual interactions the hole states are not eigenstates of the residual nucleus but are mixtures of several single-particle states. The latter leads to the spreading of the shell structure and requires studies of the spectral function using theoretical methods going beyond the MFA to describe successfully the relevant experiments. In Ref. [5] a realistic spectral function $S(p, \mathcal{E})$ has been constructed that is in agreement with the scaling function $f(\psi)$ obtained from the (e, e') data. For this purpose effects beyond MFA have been considered. The procedure included (i) the account for effects of a finite energy spread and (ii) the account for *NN* correlation effects considering single-particle momentum distributions $n_i(p)$ [that are components of $S(p, \mathcal{E})$] beyond the MFA, such as those related to the usage of natural orbitals (NO's) [12] for the single-particle wave functions and occupation numbers within methods in which short-range *NN* correlations are included. For the latter the Jastrow correlation method [13] has been considered. Also, in Ref. [5] FSI were accounted for using complex optical potential that has given a spectral function $S(p, \mathcal{E})$, leading to asymmetric scaling function in accordance with the experimental analysis, thus showing the essential role of the FSI in the description of electron scattering reactions.

In Figure 1 of Ref. [2] the results for the superscaling function $f(\psi)$ within the HO+FSI and NO+FSI models are presented. Accounting for FSI leads to a redistribution of the strength, with lower values of the scaling function at the maximum and an asymmetric shape around the peak position, *viz.,* when $\psi = 0$. Also, we see that the asymmetry in the superscaling function gets larger by using the Lorentzian function for the energy dependence of the spectral function than by using the Gaussian function [2, 5]. The two spectral function models, including FSI, clearly give a much more realistic representation of the data than the relativistic Fermi gas.

The third model, SuSAv2, that is an improved version of the superscaling prescription, called SuSAv2 [14], has been developed by incorporating relativistic mean field (RMF) effects [15–17] in the longitudinal and transverse nuclear responses, as well as in the isovector and isoscalar channels. This is of great interest in order to describe CC neutrino reactions that are purely isovector. Note that in this approach the enhancement of the transverse nuclear response emerges naturally from the RMF theory as a genuine relativistic effect.

The detailed description of the SuSAv2 model can be found in [14, 18, 19]. Here we just mention that it has been validated against all existing (e, e') data sets on ^{12}C, yielding excellent agreement over the full range of kinematics spanned by experiments, except for the very low energy and momentum transfers, where all approaches based on impulse approximation (IA) are bound to fail. Furthermore, the success of the model depends on the inclusion of effects associated with two-body electroweak currents, which will be briefly discussed in the next Section.

Ingredients beyond the impulse approximation (IA), namely 2p-2h MEC effects, are essential in order to explain the neutrino-nucleus cross sections of interest for neutrino oscillation experiments. Following previous works [18–21], here we make use of a general parametrization of the MEC responses that significantly reduces the computational time. Its functional form for the cases of ^{12}C and ^{16}O is given in [18, 19, 22], and its validity has been clearly substantiated by comparing its predictions with the complete relativistic calculation.

3 Charge-Current QE (Anti)Neutrino Scattering on ^{12}C

In this section we show the predictions of the two spectral function approaches previously described, HO and NO, both including FSI and 2p–2h MEC. We compare the results with data from three different experiments: MiniBooNE, MINERνA and T2K. Our study is restricted to the QE-like regime where the impulse approximation in addition to the effects linked to the 2p-2h meson-exchange currents play the major role. We follow closely the general analysis presented in [19] for the case of the superscaling approach. Hence, for reference, we compare our new theoretical predictions with the results corresponding to the SuSAv2-MEC model.

The predicted ν_μ and $\overline{\nu}_\mu$ fluxes at the MiniBooNE [23], MINERνA [24] and T2K [25] detectors and corresponding mean energies are compared in Figure 1. $\Phi_{\rm tot}$ is the total integrated ν_μ ($\overline{\nu}_\mu$) flux factor: $\Phi_{\rm tot} = \int \Phi(\varepsilon) d\varepsilon$, where ε is incident beam energy. As observed, the neutrino and antineutrino mean energies corresponding to MiniBooNE and T2K experiments are rather similar, although the T2K energy flux shows a much narrower distribution. This explains the different role played by 2p-2h MEC effects in the two cases, these being larger for MiniBooNE (see [19] and results in next sections). On the contrary, the MINERνA energy flux is much more extended to higher energies, with an average value close to $3.5 - 4.0$ GeV.

3.1 MiniBooNE

In Figure 2 results are presented for the MiniBooNE flux averaged CCQE ν_μ–^{12}C ($\overline{\nu}_\mu$–^{12}C) single differential cross section per nucleon as a function of the muon kinetic energy [left panels – (a) and (c)] and of the muon scattering angle [right panels – (b) and (d)]. The top panels [(a) and (b)] correspond to neutrino

cross sections and the bottom [(c) and (d)] ones to antineutrino reactions. Theoretical predictions including both the QE and the 2p-2h MEC contributions are in

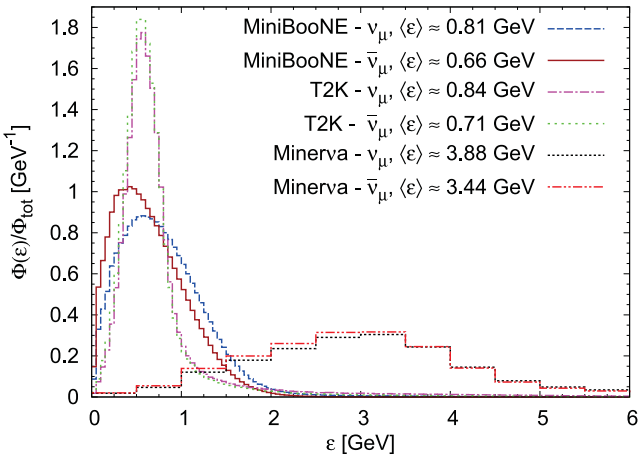

Figure 1. The predicted ν_μ ($\overline{\nu}_\mu$) fluxes at the MiniBooNE [23], MINERνA [24] and T2K [25] detectors and corresponding mean energies.

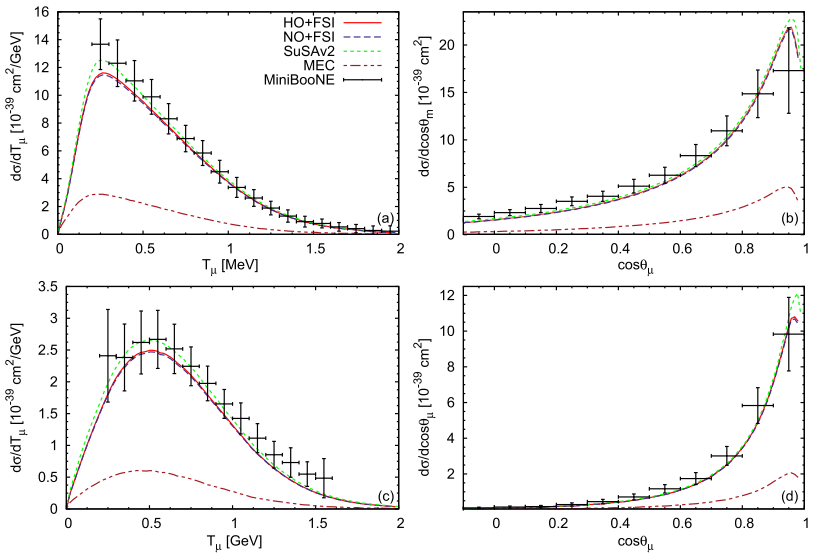

Figure 2. MiniBooNE flux-averaged CCQE ν_μ–^{12}C ($\overline{\nu}_\mu$–^{12}C) differential cross section per nucleon as a function of the muon scattering angle [left panels – (a) and (c)] and of the muon kinetic energy [right panels – (b) and (d)]. The top panels [(a) and (b)] correspond to neutrino cross sections and the bottom [(c) and (d)] ones to antineutrino reactions. The data are from [26, 27].

good accord with the data. With regard to the comparison between the different models, we observe that HO+FSI and NO+FSI provide very close responses in all kinematical situations for neutrinos and antineutrinos: the inclusive cross section is not sensitive to the details of the spectral function. HO+FSI and NO+FSI lead to almost identical cross sections that differ from the SuSAv2 prediction by less than $\sim 5\% - 7\%$ at the maximum. The important contribution linked to the 2p-2h MEC (of the order of $\sim 20\% - 25\%$ of the total response) is clearly seen to be essential in order to describe the data. More results can be found in Ref. [4].

3.2 T2K

In Figure 3 we present the flux-averaged double differential cross sections corresponding to the T2K experiment [28]. The graphs are plotted against the muon momentum, and each panel corresponds to a bin in the scattering angle. As in the previous case, we show results obtained within the SuSAv2, HO+FSI, and NO+FSI approaches including MEC and also the separate contributions of the 2p-2h MEC. As already pointed out in [19], the narrower T2K flux, sharply peaked at about 0.7 GeV (see Figure 1), is the reason of the smaller contribution provided by the 2p-2h MEC (of the order of $\sim 10\%$) as compared with the MiniBooNE results: in fact, the main contribution for the 2p-2h response comes from momentum transfers $q \sim 500$ MeV, which are less important at T2K kinemat-

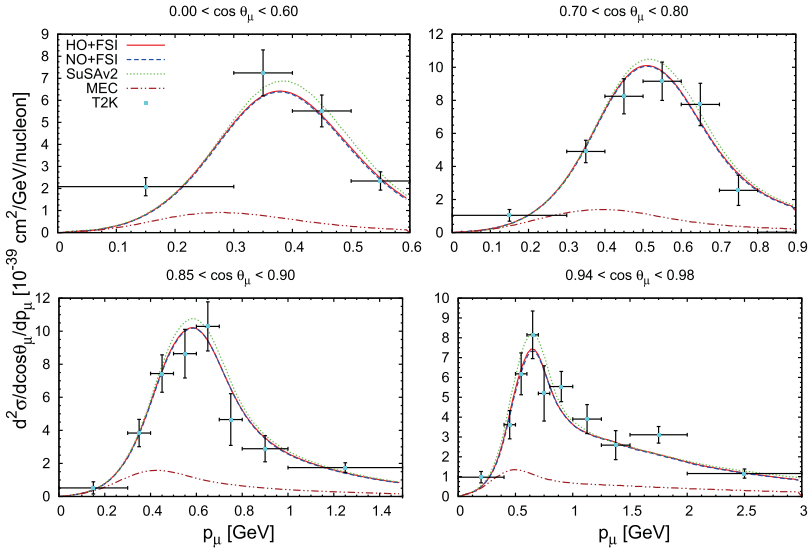

Figure 3. T2K flux-folded double differential cross section per target nucleon for the ν_μ CCQE process on ^{12}C displayed versus the μ^- momentum p_μ for various bins of $\cos\theta_\mu$ obtained within the SuSAv2, HO+FSI, and NO+FSI approaches including MEC. MEC results are shown also separately. The data are from [28].

ics. Concerning the theoretical predictions, the two SF models produce almost identical cross sections that deviate from SuSAv2, particularly at very forward scattering (right-bottom panel).

In the particular case of the most forward scattering kinematics (bottom panel on the right), notice that SuSAv2 cross section at the maximum exceeds SF+FSI results by $\sim 30\% - 35\%$. However, the large error bands shown by T2K data do not allow us to discriminate between the different models, *i.e.,* neither between pure QE calculations nor global QE+2p-2h MEC results. Furthermore, notice that the cross section reaches an almost constant value, different from zero, as p_μ increases. This is in contrast with all remaining situations explored in the previous figures.

3.3 MINERνA

In Figure 4 we show the double differential cross section of muonic antineutrino on hydrocarbon as a function of the transverse (with respect to the antineutrino beam) momentum of the outgoing muon, in bins of the muon longitudinal momentum. As shown, the spread in the results ascribed to the three models used is small, of the order of $\sim 5\% - 6\%$ at the maximum. On the other hand, we note the excellent agreement between the theory and data once 2p-2h MEC effects ($\sim 20\% - 30\%$ at the maximum) are included. This significant contribution of

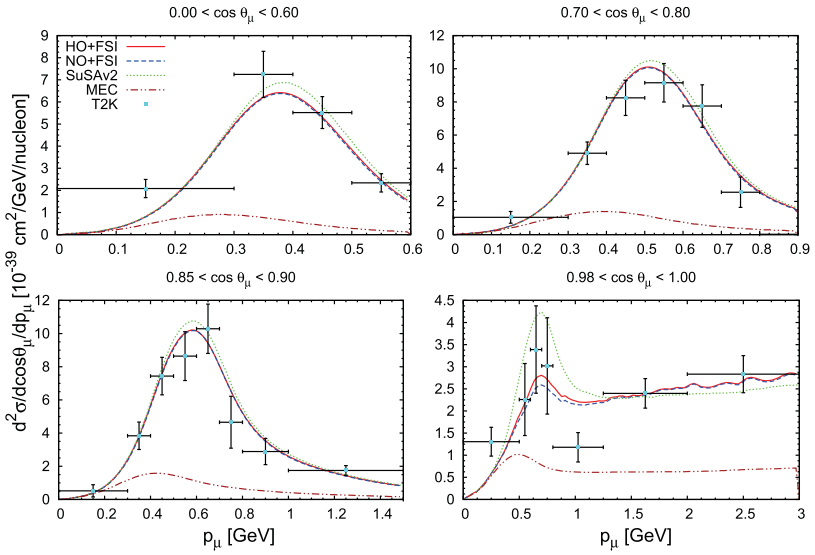

Figure 4. The MINERνA "QE-like" double differential cross sections for $\overline{\nu}_\mu$ scattering on hydrocarbon versus the muon transverse momentum, in bins of the muon longitudinal momentum (in GeV). The data are from Ref. [29].

the 2p-2h MEC effects is consistent with the results observed for MiniBooNE in spite of the very different muon antineutrino energy flux in the two experiments.

4 Neutral-Current QE Neutrino Scattering on ^{12}C

In this section the theoretical predictions of the RFG, HO+FSI, NO+FSI, SUSA scaling functions are compared with the data measured by the MiniBooNE and BNL Collaborations. The comparison is performed also with the results of the RMF and RGF models, which are based on the same relativistic mean-field model for nuclear structure but on a different treatment of FSI. In the RMF model FSI are described by the same relativistic mean field potential describing the initial nucleon state; the description of FSI in the RGF is based on the use of a complex optical potential. Details of the RGF model can be found, for instance, in [34, 35]. The results of the RMF and RGF models have been already

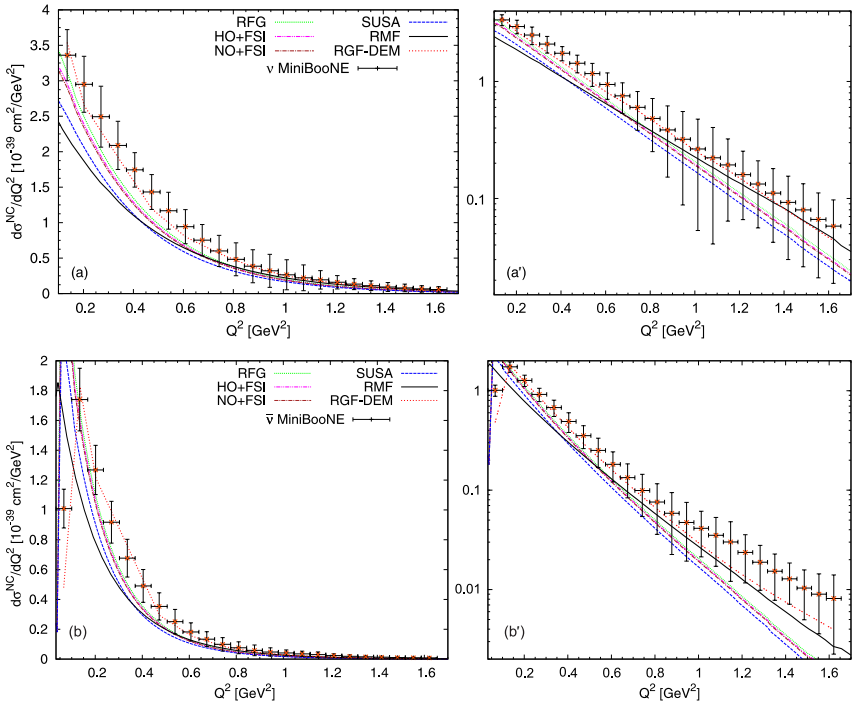

Figure 5. NCQE neutrino [panels (a) and (a′), $\nu N \to \nu N$] and antineutrino [panels (b) and (b′), $\bar{\nu} N \to \bar{\nu} N$] flux-averaged differential cross section computed using the RFG, HO+FSI, NO+FSI, SUSA scaling functions, RGF and RMF models and compared with the MiniBooNE data [30, 31]. The results correspond to the world-average axial mass $M_A = 1.032$ GeV and strangeness $\Delta s = 0$. The error bars do not account for the normalization uncertainty of 18.1% (19.5%) in the $\nu(\bar{\nu})$ case.

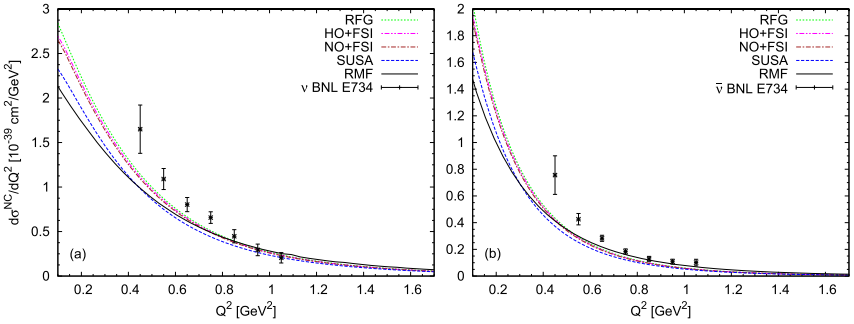

Figure 6. NCQE flux-averaged cross section: $\nu p \to \nu p$ [panel (a)] and $\bar{\nu} p \to \bar{\nu} p$ [panel (b)] compared with the BNL E734 experimental data [32, 33]. Our results are evaluated using the RFG, HO+FSI, NO+FSI, SUSA scaling functions, and RMF model with the standard value of the axial-vector dipole mass $M_A = 1.032$ GeV^2 and strangeness $\Delta s = 0$. The error bars do not include the normalization uncertainty of 11.2% (10.4%) in the $\nu(\bar{\nu})$ case.

and widely compared in [36] for the inclusive QE electron scattering, in [37, 38] for CCQE and in [39] for NCQE neutrino scattering. The RGF calculations presented in this work have been carried out with the so-called "democratic" parametrization of the optical potential of [40] (RGF-DEM).

The comparison between theory and experiment for the NCQE flux-averaged MiniBooNE (anti)neutrino cross section is presented in Figure 5. Here we compare the predictions using the RFG, HO+FSI, NO+FSI, SUSA scaling functions, and RMF model with the data. As usual in NC reactions, in this work, the variable Q^2 is defined as $Q^2 = 2M_N T_N$, where M_N and T_N are the mass and kinetic energy of the outgoing nucleon, respectively. As can be seen from Figure 5 the theoretical results corresponding to all models except the RGF-DEM underestimate the neutrino data in the region between $0.1 < Q^2 < 0.7$ GeV^2, while all theories are within the error bars for higher Q^2. On the other hand the same models underestimate the antineutrino data at high Q^2. This is clearly seen in the panels (a′) and (b′) of Figure 5, where the cross sections are represented in logarithmic scale. The RGF-DEM results are larger than the results of the other models and in generally good agreement with the data over the entire Q^2 region considered in the figure. The enhancement of the RGF cross sections is due to the contribution of final-state channels that are recovered by the imaginary part of the optical potential and that are not included in the other models.

We now compare the results obtained with our models with the BNL E734 experimental data. The mean value of neutrino (antineutrino) energy is 1.3 GeV (1.2 GeV) for BNL experiment, while for MiniBooNE experiment it is 788 MeV (665 MeV). In Figure 6 the differential cross sections evaluated using the RFG, HO+FSI, NO+FSI, SUSA scaling functions, and RMF model are compared with NCQE $\nu p \to \nu p$ [panel (a)] and $\bar{\nu} p \to \bar{\nu} p$ [panel (b)] BNL E734 experimental

data. The BNL E734 experiment was performed using a 170-metric-ton high-resolution target-detector in a horn-focused (anti)neutrino at the Brookhaven National Laboratory. The cross sections results show a behaviour similar to those of the MiniBooNE experiment. The latter (using the Cherenkov detector filled with mineral oil (CH_2)) is sensitive to both $\nu(\bar{\nu})p$ and $\nu(\bar{\nu})n$ NCQE scattering [30, 31]. It has been known for some time (see, *e.g.*, [41–43]) that the Δs-dependence of the NCQE neutrino-nucleon cross section is very mild. This results from a cancellation between the effect of Δs on the proton and neutron contributions, which are affected differently by the axial strangeness: by changing Δs from zero to a negative value the proton cross section gets enhanced while the neutron one is reduced, so that the net effect on the total cross section is very small. NCQE $\nu(\bar{\nu})p$ differential cross sections were measured in the BNL E734 experiment, which are sensitive to the values of Δs (there is not a cancellation effect). The BNL E734 experimental data can be reproduced within our models in principle by the fit of the axial strangeness without change of the axial mass value.

Here we would like to mention that, first, our calculations using NO and HO single-particle wave functions in $n_i(p)$ in the spectral function with FSI and without FSI show that the inclusion of FSI effects leads to a small change (a depletion) of the cross sections. Second, the results for the cross sections obtained using realistic spectral function $S(p, E)$ with single-particle momentum distributions $n_i(p)$ that include Jastrow short-range *NN* correlations (accounted for in the NO's) can be compared in Figures 5 and 6 with those when *NN* correlation are not included (RFG and HO). It can be seen that, similarly to the case of CCQE neutrino scattering (see Ref. [2]), the differences between results in correlated and non-correlated approaches are small, thus showing that the process is not too sensitive to the specific treatment of the bound state.

5 Conclusions

The main objective of this work is centered in the use of a realistic spectral function, that accounts for short-range *NN* correlations, and has also a realistic energy dependence. This function gives a scaling function in accordance with electron scattering data and it can be used for a wide range of neutrino energies. Therefore, the use of this spectral function to describe the general reaction mechanism involved in CC and NC neutrino-nucleus scattering processes can provide very valuable information that can be confronted with results obtained with other theoretical approaches. In this sense, we compare our spectral function-based predictions with the results provided by the SuSA, SuSAv2, RMF and RGF models largely used by us in the past. The discrepancies found can help disentangling effects directly linked to particular ingredients in the process: final state interactions, nucleon correlations, effects beyond the impulse approximation, *etc.*

An interesting outcome of the present study is that the results obtained with the NO spectral function, which accounts for *NN* short-range Jastrow correlations, are very similar to those obtained with the uncorrelated HO spectral function, thus indicating that the role played by this type of correlations is very minor for the observables analyzed in this study. The results of CC quasielastic (anti)neutrino scattering, shown in this work, can be considered as a test of the reliability of the present spectral function based models. They compare extremely well with the SuSAv2 approach, based on the phenomenology of electron scattering data, although they fail in reproducing neutrino (antineutrino) scattering data unless ingredients beyond the impulse approximation are incorporated. The present study gives us confidence in extending the use of these models to other processes, such as semi-inclusive CCν reactions and neutral current processes.

Acknowledgements

This work was partially supported by the Bulgarian National Science Fund under Contract No. KP-06-N38/1.

References

[1] L. Alvarez-Ruso *et al.*, *Prog. Part. Nucl. Phys.* **100** (2018) 1.
[2] M.V. Ivanov *et al.*, *Phys. Rev. C* **89** (2014) 014607.
[3] M.V. Ivanov *et al.*, *Phys. Rev. C* **91** (2015) 034607.
[4] M.V. Ivanov *et al.*, *Phys. Rev. C* **99** (2019) 014610.
[5] A.N. Antonov *et al.*, *Phys. Rev. C* **83** (2011) 045504.
[6] I.R. Simo *et al.*, *Phys. Rev. D* **90** (2014) 033012.
[7] I. Ruiz Simo *et al.*, *J. Phys.* **G44** (2017) 065105.
[8] I.R. Simo *et al.*, *Phys. Rev. C* **94** (2016) 054610.
[9] J.E. Amaro *et al.*, *Phys. Rev. C* **71** (2005) 015501.
[10] M. Barbaro *et al.*, *Nuclear Physics A* **643** (1998) 137.
[11] J.A. Caballero *et al.*, *Phys. Rev. C* **81** (2010) 055502.
[12] P.-O. Löwdin, *Phys. Rev.* **97** (1955) 1474.
[13] M.V. Stoitsov, A.N. Antonov, S.S. Dimitrova, *Phys. Rev. C* **48** (1993) 74.
[14] R. González-Jiménez *et al.*, *Phys. Rev. C* **90** (2014) 035501.
[15] J.A. Caballero *et al.*, *Phys. Rev. Lett.* **95** (2005) 252502.
[16] J.A. Caballero, *Phys. Rev. C* **74** (2006) 015502.
[17] J. Caballero *et al.*, *Physics Letters B* **653** (2007) 366.
[18] G.D. Megias *et al.*, *Phys. Rev. D* **94** (2016) 013012.
[19] G.D. Megias *et al.*, *Phys. Rev. D* **94** (2016) 093004.
[20] G.D. Megias *et al.*, *Phys. Rev. D* **91** (2015) 073004.
[21] M.V. Ivanov *et al.*, *J. Phys. G: Nucl. Part. Phys.* **43** (2016) 045101.
[22] G.D. Megias *et al.*, *J. Phys. G: Nucl. Part. Phys.* **46** (2018) 015104.
[23] A.A. Aguilar-Arevalo *et al.*, (MiniBooNE Collaboration), *Phys. Rev. D* **79** (2009) 072002.

[24] L. Aliaga *et al.*, (MINERνA Collaboration), *Phys. Rev. D* **94** (2016) 092005.
[25] K. Abe *et al.*, (T2K Collaboration), *Phys. Rev. D* **87** (2013) 012001.
[26] A.A. Aguilar-Arevalo *et al.*, (MiniBooNE Collaboration), *Phys. Rev. D* **81** (2010) 092005.
[27] A.A. Aguilar-Arevalo *et al.*, (MiniBooNE Collaboration), *Phys. Rev. D* **88** (2013) 032001.
[28] K. Abe *et al.*, (T2K Collaboration), *Phys. Rev. D* **93** (2016) 112012.
[29] C.E. Patrick *et al.*, (MINERνA Collaboration), *Phys. Rev. D* **97** (2018) 052002.
[30] A.A. Aguilar-Arevalo *et al.*, (MiniBooNE Collaboration), *Phys. Rev. D* **82** (2010) 092005.
[31] A.A. Aguilar-Arevalo *et al.*, (MiniBooNE Collaboration), *Phys. Rev. D* **91** (2015) 012004.
[32] K. Abe *et al.*, *Phys. Rev. Lett.* **56** (1986) 1107.
[33] L.A. Ahrens *et al.*, *Phys. Rev. D* **35** (1987) 785.
[34] F. Capuzzi *et al.*, *Nucl. Phys. A* **524** (1991) 681.
[35] A. Meucci *et al.*, *Phys. Rev. C* **67** (2003) 054601.
[36] A. Meucci *et al.*, *Phys. Rev. C* **80** (2009) 024605.
[37] A. Meucci *et al.*, *Phys. Rev. Lett.* **107** (2011) 172501.
[38] A. Meucci *et al.*, *Phys. Rev. C* **83** (2011) 064614.
[39] C. Maieron, T.W. Donnelly, I. Sick, *Phys. Rev. C* **65** (2002) 025502.
[40] E.D. Cooper *et al.*, *Phys. Rev. C* **80** (2009) 034605.
[41] W.M. Alberico *et al.*, *Nucl. Phys. A* **623** (1997) 471.
[42] W.M. Alberico *et al.*, *Nucl. Phys. A* **651** (1999) 277.
[43] M.B. Barbaro *et al.*, *Phys. Rev. C* **54** (1996) 1954.